Journal of the Electrochemical Society

SO_3 Treatment of Lithium- and Manganese-Rich NCMs for Li-Ion Batteries: Enhanced Robustness towards Humid Ambient Air and Improved Full-Cell Performance

To cite this article: Johannes Sicklinger *et al* 2020 *J. Electrochem. Soc.* **167** 130507

Journal of The Electrochemical Society, 2020 **167** 130507

SO_3 Treatment of Lithium- and Manganese-Rich NCMs for Li-Ion Batteries: Enhanced Robustness towards Humid Ambient Air and Improved Full-Cell Performance

Johannes Sicklinger,[*] Hans Beyer,[z] Louis Hartmann,[*] Felix Riewald, Christian Sedlmeier, and Hubert A. Gasteiger[**]

Chair of Technical Electrochemistry, Department of Chemistry and Catalysis Research Center, Technische Universität München, D-85748 Garching, Germany

To increase the specific capacity of layered transition metal oxide based cathode active materials (CAMs) for Li-ion batteries such as NCMs ($Li(Ni_xCo_yMn_z)O_2$, with x + y + z = 1), two major strategies are pursued: (i) increasing the Ni content (beyond, e.g., NCM811 with x = 0.8 and y = z = 0.1) or (ii) using Li- and Mn-rich NCMs (LMR-NCMs) which can be represented by the formula x $Li_2MnO_3 \cdot (1-x)$ $LiNi_xCo_yMn_zO_2$. Unfortunately, these materials strongly react with CO_2 and moisture in the ambient: Ni-rich NCMs due to the high reactivity of nickel, and LMR-NCMs due to their ≈10-fold higher specific surface area. Here we present a novel surface stabilization approach via SO_3 thermal treatment of LMR-NCM suitable to be implemented in CAM manufacturing. Infrared spectroscopy and X-ray photoelectron spectroscopy prove that SO_3 treatment results in a sulfate surface layer, which reduces the formation of surface carbonates and hydroxides during ambient air storage. In contrast to untreated LMR-NCM, the SO_3-treated material is very robust towards exposure to ambient air at high relative humidity, as demonstrated by its lower reactivity with ethylene carbonate based electrolyte (determined via on-line mass spectrometry) and by its reduced impedance build-up and improved rate capability in full-cell cycling experiments.

 [DOI: 10.1149/1945-7111/abb6cb]

Manuscript submitted June 26, 2020; revised manuscript received September 1, 2020. Published September 18, 2020. *This was paper 235 presented at the Cancun, Mexico, Meeting of the Society, September 30-October 4, 2018.*

Supplementary material for this article is available online

Li-ion battery cathode active materials (CAMs) currently considered for battery electric vehicle applications include NCA (e.g., $LiNi_{0.80}Co_{0.15}Al_{0.05}O_2$) and NCMs ($Li(Ni_xCo_yMn_z)O_2$, with $x + y + z = 1$).[1] Two of the main strategies to further increase their specific energy density are increasing the nickel as well as the development of lithium- and manganese-rich NCMs (LMR-NCMs) with the composition $xLi_2MnO_3 \cdot (1-x)LiNi_xCo_yMn_zO_2$, whereby the advantage of the latter would not only be its lower cost (due to a low nickel content) but also its significantly higher capacity.[1–4] One drawback of higher nickel contents is the increased reactivity with moisture and CO_2 from ambient air, as described in several studies in the literature.[5–9] In case of LMR-NCMs, their typically ≈10-fold higher specific surface area compared to NCMs[10] gives rise to a large number of reactive surface sites forming surface contaminants when exposed to ambient air. Recently, there has been a number of studies on the surface contamination of NCM cathode materials.[9,11–13] The reactivity of layered transition metal oxides such as $LiNiO_2$ and $LiNi_{0.5}Co_{0.5}O_2$ with moisture and CO_2 has already been discussed in earlier studies[8,14] as well as in the patent literature.[15–20] When Ni-rich or LMR-NCM are exposed to ambient atmosphere, CO_2 and H_2O readily react with the particle surface forming carbonates, hydroxides and hydrates.[7,8,13,21,22] These surface species lead to electrolyte decomposition, gassing, impedance buildup, and ultimately deteriorated cycle-life.[1,5,7,8,11–13,21–25] In addition, these basic species can trigger gelation[26] of NMP-based slurries, which complicates the electrode coating process. The most straightforward strategy to prevent such adverse effects is to avoid any exposure to moisture and CO_2 after material synthesis, which, however, is challenging in a large-scale industrial process. Thus it would be highly advantageous to add a step to the CAM manufacturing process which makes them robust against exposure to ambient atmosphere in order to facilitate storage, large-scale ink processing, and electrode manufacturing. For this, the reactive sites on the surface of nickel-rich NCMs or on LMR-NCMs with very high specific surface areas which react with CO_2 and/or H_2O must be removed prior to any potential exposure of the materials to ambient atmosphere.

Several approaches to stabilize the surface of layered transition metal oxides have been explored in the literature. These are, for example, wet chemical processes to produce spinel surface coatings on LMR-NCM[27] as well as on NCM[28] or surface modifications of LMR-NCMs by TiO_2, Al_2O_3, or AlF_3 coatings.[29,30] None of these studies, however discuss the impact of these modifications on the chemical stability of the modified CAMs towards CO_2 and moisture. In our here presented study, we aim to convert the reactive surface groups of LMR-NMC into less reactive sulfate species in order to induce chemical stability of the CAM particles towards ambient air. The generation of a Na_2SO_4 surface layer has been reported using sodium dodecyl sulfate as a precursor, however without investigating the ambient storage stability.[31] In the patent literature, the addition of sodium thiosulfate and sodium dodecyl sulfate to an aqueous washing solution in order to reduce gas generation in pouch cells was reported for NCA.[32] An alternative route to surface sulfation is mixing the cathode active material with $Na_2S_2O_8$ powder, either in the dry state or by spray coating, as described in the patent literature.[19] Yet another approach found in the literature is covering the surface of NCM811 particles with sulfated zirconia, which is demonstrated to have a positive impact on cycling, again without investigating the stability of the material upon exposure to ambient air.[33] In addition, Chae and Yim[34] reported the generation of an SO_x-immobilized surface layer on Ni-rich NCM particles via a wet-chemical approach based on a sulfate surfactant. The improved cycling performance of the coated particles was explained by the mitigation of side reactions with the electrolyte. The drawback of all these surface coating approaches is that they are batch treatments with limited scalability, while for industrial CAM manufacturing a continuous process would be advantageous. In the study at hand we present a novel approach for surface sulfation of layered transition metal oxides, i.e., a thermal treatment with SO_3 gas. Recently, we

*Electrochemical Society Student Member.
**Electrochemical Society Fellow.
[z]E-mail: hans.beyer@tum.de

have also studied surface passivation with SO_2 gas[35] in collaboration with the Aurbach group at Bar-Ilan University in Israel. Treatments of cathode active materials with various reactive gases including SO_2 and SO_3 are also described in our recent patent application[36] in collaboration with Bar-Ilan University and BASF. Therein, SO_2 was shown to enhance full-cell cycling performance of LMR-NCM as well as reduce CO_2 gassing by forming sulfur species on the CAM particle surface.[36] A prior patent application by Watanabe and Deguchi describes the reactive gas treatment of calendared NCM-based cathode sheets and claims that Li_2SO_4 formed due to the SO_2 treatment can lower the CO_2 gas generation from the decomposition reactions of the electrolyte solution.[37]

Here, we explore a chemical surface modification by an SO_3 gas treatment that would be well-suited for implementation in an industrial manufacturing process for layered transition metal oxide based CAMs, as schematically shown in Fig. 1. The synthesis of NCM or LMR-NCM was discussed in greater detail in our recent study on surface contaminants.[13] In brief, transition metal precursors, mixed transition metal sulfates or nitrates,[16,17] are mixed with a lithium precursor (Li_2CO_3 or a $LiOH{\cdot}H_2O$).[15,16] The mixture is subsequently calcined under O_2-containing atmosphere, e.g., in a pusher kiln (step 1 in Fig. 1) to form the desired layered transition metal oxide CAM. During hydroxide or carbonate decomposition, H_2O and CO_2 are formed; during the subsequent cool-down (step 2), dry atmosphere is supplied to remove this H_2O and CO_2, which would otherwise lead to the formation of surface hydroxides and carbonates. Our proposed surface passivation procedure could easily be added to this established process as step 3: after cool-down to the desired treatment temperature of 160 °C or 200 °C, 0.5% SO_3 is added to a dry carrier-gas stream to react with the layered oxide particle surface, converting reactive species such as residual lithium ($LiOH$, $LiOH \cdot H_2O$, Li_2CO_3) or nickel carbonate-hydroxides (such as $(NiCO_3)_2 \bullet (Ni(OH)_2)_3 \bullet 4\ H_2O$)[13] on the surface of the LMR-NCM or its oxide surface groups into passivating sulfate species. The goal of this surface modification approach is to enable the subsequent exposure of LMR-NCM to CO_2 and H_2O (step 4) without forming surface contaminants.

To mimic the proposed surface modification approach on the lab scale, we re-calcine the as-received LMR-NCM at 625 °C in O_2/Ar atmosphere inside a tube furnace with controlled gas flow to remove any contaminants that may have formed unintentionally during shipping and storage. After cool-down to 160 °C or 200 °C, we add 0.5% SO_3 to the gas stream. The reactive SO_3 gas is continuously generated by the so-called contact process, viz., by SO_2 oxidation at elevated temperature in a fixed-bed tube reactor filled with a V_2O_5 catalyst (see experimental section for details). We use Diffusive Reflectance Infrared Fourier Transform Spectroscopy (DRIFTS) and X-ray Photoelectron Spectroscopy (XPS) to demonstrate that this treatment leads to the formation of surface sulfates. Furthermore, we study the chemical reactivity of LMR-NCM at 60 °C with ethylene carbonate (EC) based electrolyte by On-line Mass Spectrometry (OMS), comparing SO_3-treated and untreated LMR-NCM. To assess the practical implications of our surface modification approach on full-cell cycling, we test LMR-NCM//graphite coin cells at an elevated temperature of 45 °C. In our previous work,[13] we already demonstrated that the combined DRIFTS, XPS, OMS and electrochemical analysis represents a powerful toolbox to assess surface contamination of layered transition metal oxides. In this work, we extend the use of this toolbox to characterize SO_3-treated LMR-NCM surfaces and their behavior during ambient storage at high-humidity.

Experimental

Processing of cathode active materials.—LMR-NCM was provided by BASF, shipped under inert packaging, and stored in an Ar-filled glovebox (O_2, $H_2O < 0.1$ ppm, MBraun, Germany). As in previous studies from our group,[10,38] $Li_{1.17}[Ni_{0.22}Co_{0.12}Mn_{0.66}]_{0.83}O_2$, which can also be written as $0.42\ li_2MnO_3 \cdot 0.58\ li[Ni_{0.38}Co_{0.21}Mn_{0.41}]O_2$ was used for all experiments in this study (with a BET area of $\approx$6.5 $m^2\ g^{-1}$). To establish a well-defined initial state of the LMR-NCM material, the as-received material was dried using the same conditions as for electrodes, i.e., 12 h at 120 °C under dynamic vacuum in a glass oven (Büchi, Switzerland). This sample is referred to as "dry" (see Fig. 2, gray box). The "calcined" sample (black box) was obtained by heat treatment of the "dry" material in a tube furnace (Carbolite, Germany) for 1 h at 625 °C (ramp: 10 K min^{-1}) in a mixture of 30% O_2 and 70% Ar (99.999% purity, Westfalen, Germany) with a controlled gas flow of 1 l min^{-1}. This calcination method was also included as a first step in our surface modification procedure (orange

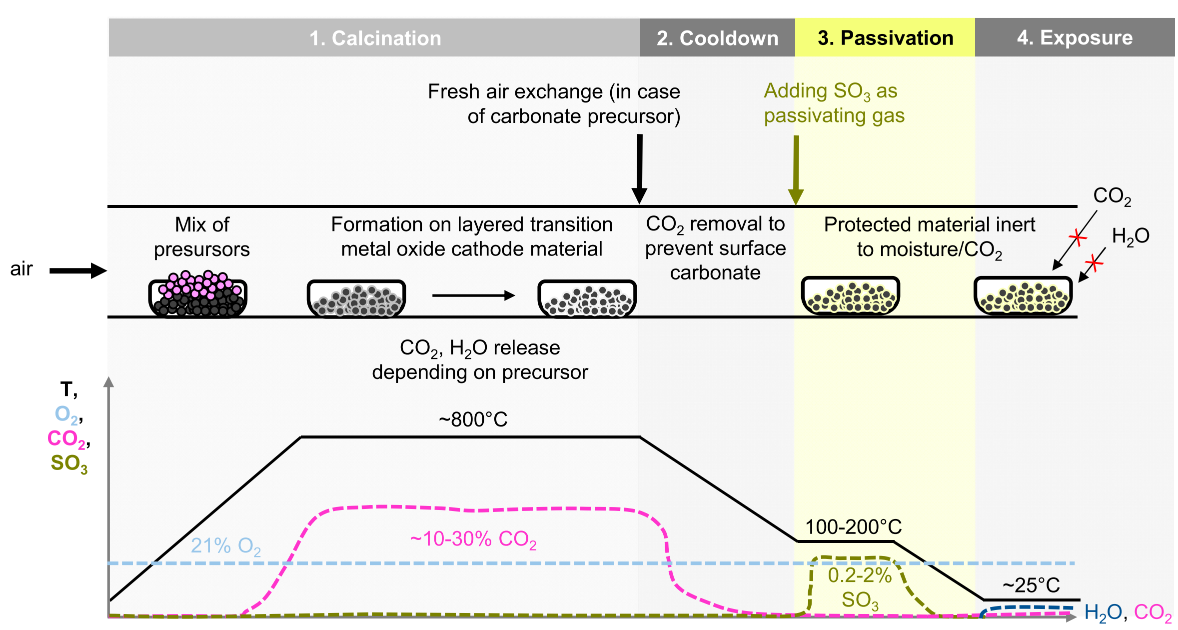

Figure 1. Process scheme for industrial manufacturing of LMR-NCMs. The precursor mix consists of LiOH or Li_2CO_3 salt mixed with transition metal carbonates (similar scheme can be found in our recent article on NCM811 and NCM111).[13] The here proposed surface passivation step (step 3) is highlighted in yellow, while the subsequent exposure test to ambient air at high relative humidity is sketched in step 4.

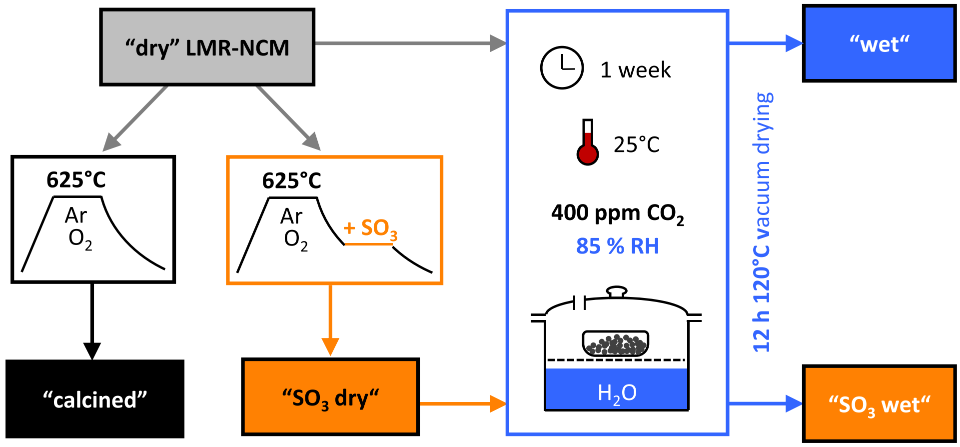

Figure 2. Depiction of the various treatments applied to the LMR-NCM material and labeling scheme of the differently treated samples that is used throughout this manuscript: i) "dry" refers to the as-received LMR-NCM material after 12 h drying under dynamic vacuum at 120 °C; ii) "calcined" refers to this material after calcination in 30% O_2/Ar at 625 °C for 1 h; iii) "SO_3 dry" refers to LMR-NCM after calcination and subsequent treatment with 0.5% SO_3 at 160 °C or 200 °C; iv) "wet" and "SO_3 wet" refers to the "dry" and "SO_3 dry" LMR-NCM materials, respectively, after they had been stored at high-humidity ambient air.

box): first, the sample was calcined in 30% O_2/Ar at 625 °C as for the "calcined" sample; then, after cool-down to the desired SO_3 treatment temperature, the sample was treated for 1 h at either 160 °C or 200 °C by adding 0.5% SO_3 to the 30% O_2/Ar gas mixture. These SO_3-treated (referred to as "SO_3 dry") as well as the "calcined" samples were transferred to the glovebox under inert conditions after cool down in 30% O_2/Ar (1 l min^{-1}).

SO_3 was produced by oxidation of SO_2 via the industrially established contact process[39,40] conducted in a vertically aligned tube reactor made in-house. As mentioned in the introduction, SO_2 had been investigated in a previous study,[35] while the paper at hand discusses the impact of SO_3 treatment on LMR-NCM. The reactor consists of a ceramic tube (l = 1100 mm, $\varnothing_i$ = 12 mm, $\varnothing_o$ = 16 mm, made of Degussit AL23, Friatec, Germany), jacketed by a wound electric heating wire (l = 3,0 m, P = 350 W, Horst, Germany) that results in a heated tube length of 50 cm, a temperature sensor (Horst, Germany), and several layers of insulating ceramic fiber mats (Carbolite, Germany). The heated section of the reactor was filled with a V_2O_5 catalyst (Katalysator O4-111, BASF, Germany, original star-shaped pellets that were crushed to fit into the reactor tube) and preheated to 430 °C in an Ar (99.999%, Westfalen, Germany) flow. At 430 °C, a gas mixture of 0.5% SO_2 (99.98% purity, with <10 ppmv H_2SO_4 and <50 ppmv H_2O, Air Liquide, Germany) 30% O_2 (99.999%, Westfalen, Germany), and 69.5% Ar was fed to the reactor from the bottom end at a space velocity of 11/h corresponding to a total flow rate of 1 l min^{-1} when assuming a space filling of 50% by the catalyst. These conditions are recommended by the catalyst manufacturer to achieve a maximum conversion of SO_2 to SO_3. According to the directions for use provided by the catalyst manufacturer, the conversion from SO_2 to SO_3 is >97% at the given conditions. From the top end of the reactor, the product gas mixture (consisting of SO_3, O_2, Ar, and residual traces of SO_2) was fed to the above-described tube furnace containing the sample via a stainless steel gas line (Swagelok, USA). The overall setup to conduct the here described SO_3 treatment procedure is illustrated in Fig. 3.

The LMR-NCM samples referred to as "wet" and "SO_3 wet" in Fig. 2 (right-hand-side) were obtained by storing the "dry" and the "SO_3 dry" LMR-NCM samples, respectively, for one week in ambient air that was humidified over a water bath at 25 °C, thus exposing them to moisture (relative humidity of 85 ± 5%, as determined by a relative humidity sensor) and the typical concentration of ≈400 ppm CO_2 in air (analogous to our previous study on the formation of surface contaminants[13]). In more detail, the water bath was covered with a lid with a small hole to ensure moisture saturation on the one hand and to allow for the diffusion of CO_2 from the ambient air into the vessel. After "wet" storage, the samples were dried in a glass oven (Büchi, Switzerland) for 12 h at 120 °C under dynamic vacuum in order to remove physisorbed H_2O; subsequently, they were stored in an Ar-filled glovebox (<0.1 ppm O_2 and H_2O, MBraun, Germany) without exposure to ambient air after drying.

We have refrained from conducting wet storage experiments with the as-received LMR-NCM (referred to as "dry") after a subsequent calcination (marked as "calcined" in the black box of Fig. 2), as we believe that the effect of wet storage is essentially identical for the as-received "dry" LMR-NCM as it would be for the "calcined" LMR-NCM, since the as-received material has already undergone calcination at ⩾800°C during manufacturing, which still does not prevent it from rapidly accumulating surface contaminants (as will be shown below).

Diffuse reflectance infrared fourier transform spectroscopy (DRIFTS).—Infrared spectroscopy in diffusive reflectance mode (DRIFTS) is sensitive to infrared active species at the surface of particulate materials. DRIFTS spectra were recorded by an IR spectrometer (Cary 670, Agilent, USA) using the Praying Mantis (Harricks, USA) mirror optics that collects diffusively scattered IR radiation from the sample. Mixtures of treated and untreated LMR-NCM were prepared with 1 wt% of sample dispersed in finely ground KBr (FTIR-grade, Sigma-Aldrich, Germany, dried at 120 °C under vacuum prior to use) to characterize surface species. The sample/KBr mixture was prepared in an Ar-filled glovebox and the mixture was put in an air-tight chamber (HT reaction chamber, Harricks, UK) with IR-transparent windows (KBr single crystals, Korth Kristalle GmbH, Germany). The spectra evaluation is described in more detail in the supporting information (Fig. S1 available online at stacks.iop.org/JES/167/130507/mmedia).

X-ray photoelectron spectroscopy (XPS).—The powders were pressed to pellets ($\varnothing$ = 3 mm) inside an argon-filled glovebox using a hand press with a 3 mm die set (PIKE Technologies, USA) and mounted on an electrically insulated sample holder, which can be transferred from the glovebox into the XPS system without any air exposure using a Kratos sample transfer chamber. Samples were kept in the XPS antechamber until a pressure of ≈10^{-8} Torr was reached and were then transferred to the sample analysis chamber where the pressure was always kept below ≈10^{-9} Torr during the whole measurement period. Spectra were acquired using

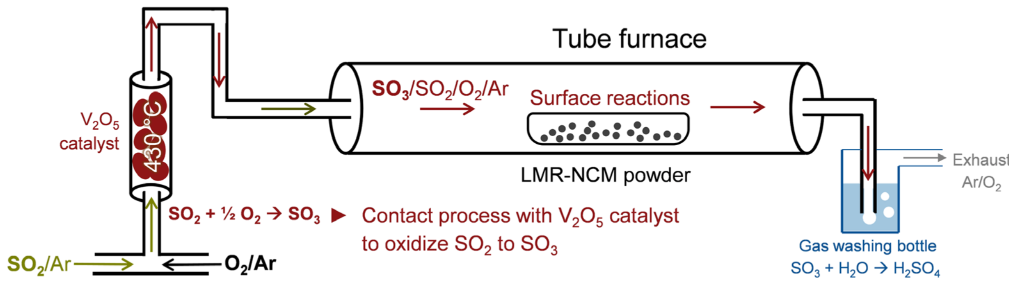

Figure 3. Detailed scheme of the tube furnace setup for the SO_3 treatment of LMR-NCM samples. On the left hand side, the contact process, i.e., the oxidation of SO_2 with O_2 over a V_2O_5 as catalyst is depicted, using a feed gas composition of 0.5% SO_2, 30% O_2, and 69.5% Ar (the latter serves as carrier gas) at a space velocity of 11/h. The gas mixture exiting the reactor and containing the highly reactive gas SO_3 then flows through the heated tube furnace, where the LMR-NCM sample is placed and where the desired reaction between SO_3 and the LMR-NCM surface takes place. The exhaust gases are quenched by a water washing bottle (on the right hand side) to avoid the emission of hazardous and corrosive SO_3.

monochromated Al Kα radiation (1486.6 eV) with an emission current of 15 mA. Survey spectra were recorded for all samples with a step size of 0.5 eV and at a pass energy of 160 eV. Detail spectra of were recorded with a step size of 0.1 eV, a pass energy of 20 eV and an emission current of 20 mA. For all measurements, a charge neutralizer was used, and the spectra were energy-calibrated to the adventitious carbon peak with a binding energy (BE) of 284.8 eV. In addition to the LMR-NCM, also the reference samples $LiSO_4$, $NiSO_4$, $NiSO_4 \cdot 6\ H_2O$, LiOH, and Li_2CO_3 (purity > 98% for all compounds, Sigma-Aldrich, Germany) were measured. A Shirley background was subtracted from all spectra. A detailed overview over the applied fitting parameters and reference spectra can be found in the supporting information.

On-line mass spectrometry (OMS).—To test the reactivity of the cathode active material with the electrolyte,[41] 515 mg of cathode active material (dried at 120 °C in vacuum overnight) were mixed with 120 μl of a model electrolyte consisting of ethylene carbonate (EC) and 1.5 M $LiClO_4$ in our OMS cell hardware,[42] resulting in an industrially relevant electrolyte to CAM mass ratio of 0.35:1.[43] For the untreated "dry" and "calcined" samples, the amounts of electrolyte and CAM were doubled. As discussed in our previous work,[13] we use the thermal decomposition of EC as a probe for the amount and the reactivity of surface contaminants present on the CAM particles, and thus selected $LiClO_4$ as an electrolyte salt that does not react with hydroxide, carbonate, or hydrate surface groups. In contrast to that, $LiPF_6$ was suggested to react with carbonates forming CO_2.[44] We are aware that our "EC-only" electrolyte is quite different to commercial electrolytes, however we have demonstrated that it is well suited model electrolyte to probe the amount of surface contaminants on NCM-based cathode active materials.[13]

Before cell assembly, all cell hardware was dried for at least 12 h at 70 °C in a vacuum oven (Thermo Scientific, USA). The sealed cell containing the CAM/electrolyte mixture was placed into a programmable controlled-temperature chamber (KB 23, Binder, Germany), and then connected to the OMS system via a crimped capillary leak ($\approx$1 μl min^{-1} gas flux into the mass spectrometer).[45] First the cell was held at 10 °C for 5 h to record a stable baseline for all ion current signals (m/z = 1 to 128). After that, the temperature was raised to 60 °C and the corresponding gas evolution was recorded for 12 h (similar to storing a lithium-ion cell at elevated temperature). The cell temperature was recorded with a thermocouple positioned in a 1 cm deep channel drilled into the stainless steel cell body. For translation of the OMS ion current signals I_z into units of [ppm], the temperature was set back to 25 °C and the cell was purged with a calibration gas containing H_2, CO, O_2, and CO_2(each at a concentration of 2000 ppm in Ar, Westfalen, Germany), by these means, one can quantify the concentrations of H_2 (m/z = 2), CO (m/z = 28), O_2 (m/z = 32), and CO_2 (m/z = 44) in the cell head space.[46]

Electrode preparation and cycling.—The cathode coating slurry was produced under inert conditions analogous to our previous study on surface contaminants,[13] i.e., mixing of the solid constituents, NMP addition, and slurry preparation were carried out in an Ar-filled glovebox inside a mixing vessel which was sealed to be air-tight before transfer out of the glovebox. To produce LMR-NCM cathodes for cycling, the following ingredients were blended together: 92.5 wt% of CAM, 4 wt% carbon black (Super C65, Timcal, Switzerland), and 3.5 wt% polyvinylidene difluoride (PVdF, Solef 5130, Solvay, Belgium). Carbon black and PVdF had been vacuum dried at 120 °C for 3 days before transfer to the glovebox. After powder mixing, 0.84 g of N-methylpyrrolidone (NMP, Sigma-Aldrich, Germany) per gram of solid (54 wt% solid content) were added in several steps, in between of which the slurry was mixed with a planetary orbital mixer (Thinky, Japan) in a sealed mixing vessel until a highly viscous, lump-free coating slurry was obtained (note that the NMP addition steps were conducted in the glovebox). The final slurry was applied onto an 18 μm thick aluminum foil (MTI, USA) with a 100 μm four-edge-blade (Erichsen, Germany) inside the glovebox and then dried overnight. Disk-shaped cathodes with a diameter of 14 mm were punched out of the foil inside the glovebox and compressed at 2.5 t for 20 s outside the glovebox. Assembly and disassembly of the compression tool were carried out inside the glovebox to keep the total time of slight air exposure below one minute. In addition, the compression tool was wrapped twice with plastic bags before transferring out of the glovebox to minimize the eventual air contact of the electrodes. After compression, the cathodes were then weighed inside the glovebox, dried overnight in a vacuum oven at 120 °C, and introduced into an Ar glovebox without exposure to ambient air. The areal loading of the LMR-NCM cathodes after drying was 5.0 ± 1.0 $mg_{LMR\text{-}NCM}/cm^2$, corresponding to an areal capacity of 1.6 ± 0.3 mAh cm^{-2} when referenced to the specific charge capacity of 320 mAh/$g_{LMR\text{-}NCM}$ for the activation in the 1st cycle. Note that the reversible capacity after activation is around 250 mAh/$g_{LMR\text{-}NCM}$.

The graphite anodes were prepared with a composition of 95 wt% T311 (SGL Carbon, Germany) and 5 wt% PVdF (Kynar HSV900, Arkema, France) under addition of 0.69 g of NMP per gram of solids (59 wt% solid content) in the same sequential mixing process as for the cathodes. The resultant coating slurry was applied onto a 12 μm thick copper foil (MTI, USA) with a 100 μm four-edge-blade (Erichsen, Germany) and then dried overnight in a convection oven at 50 °C. Disk-shaped electrodes with a diameter of 16 mm were punched out of the foil and compressed at 0.5 t for 20 s. The anodes were then weighed, dried overnight in a vacuum oven at 120 °C, and introduced into an Ar glovebox without exposure to ambient air. The areal loading of the graphite anodes after drying was 6 ± 1 $mg_{graphite}$ cm^{-2}, corresponding to an areal capacity of 1.9 ± 0.3 mAh cm^{-2} based on a specific capacity of 340 mAh/$g_{graphite}$ (corresponding to 1.5 ± 0.25 mAh cm^{-2} when referenced to the reversible LMR-NCM capacity after activation of 250 mAh/$g_{LMR\text{-}NCM}$). The thereby achieved balancing of the LMR-NCM//graphite full-cells ranges from 1:1.2 to 1:1.3 in units of [mAh cm^{-2}] referenced to the 1st charge capacity of the cells.

Electrochemical testing was conducted in CR2032 type coin cells at 45 °C with 30 μl of an electrolyte containing fluoroethylene carbonate (FEC) which already had been applied in a previous study from BASF and our group,[47] viz., FEC:DEC (12:64 v:v) with 1 M $LiPF_6$ and 24 vol% of an additional fluorinated co-solvent to improve full-cell cycling stability (BASF, Germany). Anode and cathode are separated by one polyolefin separator (Celgard H2013, USA) with 17 mm diameter. The cycling protocol is summarized in Table I and consists of the following sequence: i) a constant-current (CC) activation cycle at C/15 (segment 1), which is required to obtain the full capacity of the LMR-NCM cathode[48]; ii) three cycles at slow rate of C/10 (CC) (segment 2); iii) a DCIR (direct current internal resistance) pulse, which is a 10 s discharge pulse (C/5) at 40% SOC (state-of-charge) with simultaneous recording of the cell voltage to calculate the internal resistance (sum of all resistance contributions) using Ohm's law (segment 3); iv) three cycles at fast rate of 3 C with CCCV charging (CC charge followed by a constant-voltage hold until the current drops below C/10) and CC discharging (segment 4); and, v) 33 standard cycles with C/2 (CC) charging and 1 C (CCCV) discharging (segment 5). Segments 2–5 are repeated several times. Note that C-rates are referenced the reversible capacity of LMR-NCM after activation of 250 mAh g^{-1}.

Results

Identification of surface species on pristine and SO_3-treated LMR-NCM.—Infrared spectroscopy provides qualitative understanding of how the SO_3 treatment impacts the LMR-NCM particle surface. While Fourier Transform infrared spectroscopy (FTIR) in transmission mode is not very sensitive to surface groups on the oxide particles, Diffusive Reflectance Infrared Fourier Transform Spectroscopy (DRIFTS) is very sensitive even to low amounts of IR-active species on the particle surface, as demonstrated in our recent study on surface contaminants.[13] As described in the supporting information, all spectra are normalized to the oxide band at 570 cm^{-1}. Figure 4 contains spectra of the as-received and dried ("dry") and the SO_3-treated ("SO_3 dry") LMR-NCM. For the detailed band assignment, see Table II.

The "dry" reference sample (black line; lower-most line in Fig. 4) contains a significant amount of carbonate impurities, as indicated by the band around 1470 cm^{-1}. This asymmetrical CO_3 stretching is split into two bands due two lower symmetry of the carbonate anion at the surface compared to carbonate anions in the bulk of pure Li_2CO_3.[50] Even in case of the LMR-NCM samples that were not treated with SO_3 gas ("dry," "wet" and "calcined"; left panel), a trace amount of sulfate is detected (SO_4 stretch around 1130 cm^{-1}), which accounts for trace impurities of transition metal sulfates typically used as dissolved salts in the precipitation process to prepare the precursor in the LMR-NCM manufacturing process. Since there are no characteristic features of the sulfite ion detected, i.e., no strong band at ca. 1000 or 950 cm^{-1}(see Table II), this DRIFTS analysis gives a first hint that in contrast to sulfates, no sulfites have been formed. This is supported by the XPS analysis that will be discussed later, where we will find that SO_3 treatment exclusively leads to sulfate formation.

Since the first step of our thermal gas treatment procedure is the calcination at 625 °C, the calcined sample represents the best reference for a comparison with the SO_3-treated LMR-NCM. Indeed, after calcination (black line), the carbonate band has nearly vanished due to thermal decomposition of all surface impurities except Li_2CO_3, which in its bulk form decomposes above ≈700 °C.[65] This is of course in great contrast to "wet" LMR-NCM (turquoise line in Fig. 4), where a negative band is observed for the hydrate/hydroxide region between 2500 and 3600 cm^{-1} (minimum at 3450 cm^{-1}), which seems counterintuitive, since one would expect an upward pointing feature for infrared absorbing species. A very high concentration of surface contaminants would explain the negative shaped hydrate/hydroxide region in case of "wet" LMR-NCM.[13] In case of the carbonate band around 1470 cm^{-1}, an also frequently observed phenomenon is observed, namely a derivative shape of the DRIFTS signal, which is known to occur for highly concentrated species in DRIFTS spectroscopy.[66] "Derivative shape" means that the peak does not exclusively point in one direction, but that it is distorted in such way that it contains upward as well as downward pointing parts (best illustrated by the feature of the turquoise line near 1470 cm^{-1} in the left panel of Fig. 4), which clearly is the case for the carbonate signal of "wet" LMR-NCM. Consequently, it is safe to say that the "wet" LMR-NCM sample must have a much higher carbonate content than the "dry" and the "calcined" samples. The latter one does only have an extremely weak carbonate band and no hydroxide/hydrate signal at all.

In case of the SO_3 gas treated LMR-NCM materials, namely the "SO_3 160 °C dry" and the "SO_3 200 °C dry" samples, the intense sulfate signals at 1130 cm^{-1} including the shoulder/side band at 1160 cm^{-1} clearly prove the formation of surface sulfates over the course of the SO_3 treatment (Table II). The sulfate band intensity for the "SO_3 200 °C dry" sample is even higher compared to the "SO_3 160 °C dry" sample, indicating a higher amount of sulfate at higher SO_3 gas treatment temperature. This is consistent with XPS data, as will be discussed in the following section. The side bands at 1300 cm^{-1} and 820 cm^{-1} are likely due to either pyrosulfate groups[51–53,55–60]or to vibrational features caused by the interaction of neighboring sulfate groups on the oxide surface.

After storage of the LMR-NCM samples at ambient air with high relative humidity, both of the SO_3-treated samples ("SO_3 160 °C wet" and "SO_3 200 °C wet") exclusively exhibit upward pointing, i.e., purely absorptive bands in both the carbonate and the hydrate/hydroxide region (right panels in Fig. 4). While a derivative shape of the carbonate band around 1470 cm^{-1} was observed for the "wet" sample that was not treated with SO_3 (turquoise line in the left panel of Fig. 4), no such behavior is observed for the SO_3-treated samples after exposure to humid air ("SO_3 160 °C wet" and "SO_3 200 °C wet"), which clearly indicates that these samples contain much less hydrate and hydroxide species compared to untreated "wet" LMR-NCM, demonstrating their superior robustness against exposure to moisture. Interestingly, the sulfate stretching vibrations at

Table I. Cycling protocol for LMR-NCM//graphite coin cells at 45 °C with 30 μl of electrolyte (FEC:DEC (12:64 v:v) with 1 M $LiPF_6$ and 24 vol% of an additional fluorinated co-solvent), and one polyolefin separator (Celgard H2013, USA). Segments 2–5 are repeated 4 times and C-rates are referenced to 250 mAh/$g_{LMR\text{-}NCM}$; CC (constant-current), CCCV (constant-current constant-voltage with C/10 lower current limit), DCIR (direct current internal resistance) measurement at 40% SOC (state-of-charge), with "SOC" referring to the last discharge capacity of segment 2. The partial charge and discharge cycle directly before/after the DCIR pulse was carried out at C/10. Before the DCIR pulse (at a current corresponding to C/5) was applied, the cell was allowed to rest for 1 h in OCV mode.

	Segment	Potential range [V vs Li/Li^+]	Charge rate	Discharge rate	Cycles	Repeats
1	Activation	4.8−2.0	C/15 (CC)	C/15 (CC)	1	0
2	Slow cycling	4.7−2.0	C/10 (CC)	C/10 (CC)	3	4 (start of loop)
3	DCIR	After C/10 charge to 40% SOC and 1 h OCV	—	C/5 pulse	1	4
4	Fast cycling	4.7−2.0	C/2 (CCCV)	3 C (CC)	3	4
5	Standard cycling	4.7−2.0	C/2 (CCCV)	1 C (CC)	33	4 (end of loop)

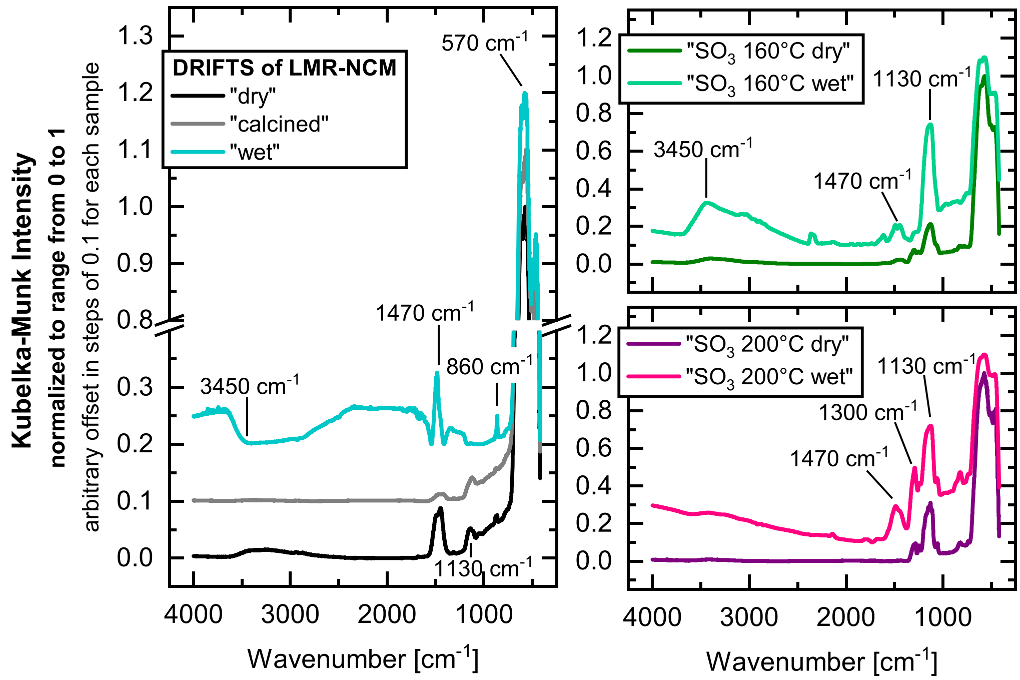

Figure 4. DRIFT spectra of the differently treated LMR-NCM samples, with the Kubelka-Munk intensity normalized to the oxide band at 570 cm^{-1} (see supporting information); the spectra are offset arbitrarily along the y-axis for better visibility. Left panel: as-received and dried LMR-NCM ("dry") as well as after calcination of the "dry" sample ("calcined") or after its wet storage ("wet"). Upper right panel: LMR-NCM treated with SO_3 at 160 °C ("SO_3 160 °C dry") and after its wet storage ("SO_3 160 °C wet"). Bottom right panel: LMR-NCM treated with SO_3 at 200 °C ("SO_3 200 °C dry") and after its wet storage ("SO_3 200 °C wet").

1130 cm^{-1} are significantly enhanced when comparing "wet" stored SO_3-treated samples to "dry" SO_3-treated samples. This could either point to an increased absorption coefficient of hydrated or protonated sulfate anions versus "free" sulfate anions or to surface rearrangements. In other words, this might indicate that SO_3 treated LMR-NCM with sulfate surface groups can still get hydrated when exposed to humidity.

The impact of SO_3 gas treatment on the surface modification of LMR-NCM and on the vulnerability of the material to "wet" storage will be discussed further in the upcoming XPS section.

In Fig. 5, S 2p spectra of pristine and SO_3-treated LMR-NCM samples can be seen. The main figure displays the data for the "200 °C SO_3" sample. According to the literature[67,68] and our reference measurements of sulfates in the supporting information (see Fig. S2), the S $2p_{3/2}$ signal of sulfates (labelled as "M-SO_4") is found at 168.7 ± 0.2 eV and is clearly detected at that position for the "200 °C SO_3" sample, while no sulfite (labelled at "M-SO_3," with S $2p_{3/2}$ at 166.8 ± 0.2 eV) or sulfide (labelled as "M-S," with S $2p_{3/2}$ at 163.0 ± 1.0 eV) can be found.[67,68] Thus it is clear that SO_3 treatment exclusively leads to the formation of sulfate groups, as was already indicated by the above DRIFTS analysis. The impact of SO_3 treatment temperature is demonstrated by the comparison of three LMR-NCM samples in the inset of Fig. 5. In case of the as-received and dried LMR-NCM ("dry"), no significant peak is visible in the S 2p spectrum, i.e., the sulfate impurities in pristine LMR-NCM, which were discussed above on the basis of the DRIFTS data, must be a rather minor amount. The LMR-NCM treated in SO_3 at 160 °C ("SO_3 160 °C dry") already exhibits a clearly marked "M-SO_4" signal, with a high peak of high intensity, which is doubled for the "SO_3 200 °C dry" sample. This clearly indicates that an increase in SO_3 treatment temperature leads to a higher amount of sulfate formed on the LMR-NCM surface. Note that we had also explored the treatment of LMR-NCM with SO_3 at a lower temperature of 120 °C, but that the M-SO_4 XPS signals in this case were so low that we decided to not examine it any further.

In the following, we will continue to discuss the surface composition of the untreated and SO_3-treated LMR-NCM samples on the basis of the XPS O 1 s data (Fig. 6).

Peak fitting of the O 1s region was performed based on literature data,[69–72] as well as reference data, i.e., O 1s spectra of Li_2SO_4, $NiSO_4$ and $NiSO_4 \cdot 6\ H_2O$ (see Fig. S2). For "dry" LMR-NCM, two distinct features can be seen, the lattice oxygen (529.2 ± 0.2 eV) labelled as 'Lattice O^{2-}' as well as hydroxide/carbonate impurities (531.3 ± 0.2 eV) labelled as "M-OH/CO_3"; details on these binding energy assignments are given in the "XPS reference data" section of the supporting information.

For the "SO_3 160 °C dry" sample, a sulfate O 1s peak labelled as "M-SO_4" appears in addition to the hydroxide/carbonate/hydroxide impurity peak, which is in line with the S 2p data. It has to be noted that the apparent increase of the "M-OH/CO_3" component in the XPS fit of the "SO_3 160 °C dry" compared to the "dry" LMR-NCM is likely due to some uncertainty in the quantitative differentiation between the hydroxide/carbonate impurities (531.3 ± 0.2 eV) and sulfate (532.0 ± 0.2 eV) signals rather than to an increase of surface impurities after the SO_3 treatment; a more quantitative analysis is unfortunately impossible, since the peak maxima are only 0.3–-0.8 eV apart from each other. This leaves two options to explain the "M-OH/CO_3" component in case of "SO_3 160 °C dry": (i) OH/CO_3 is increased compared to untreated "dry" LMR-NCM, but we cannot use the data as a proof of an increase, since the uncertainty is too big; (ii) the amount of OH/CO_3 is not increased and the signal change only reveals the uncertainty of the method. While we cannot exclude a tiny contamination with ambient air, we did not deliberately expose "SO_3 160 °C dry" LMR-NCM to ambient air or moisture, so we believe that option (ii) is more likely.

In case of the "SO_3 200 °C dry" sample, the "M-SO_4" fraction is drastically increased, which is again in line with the S 2p data shown in Fig. 5. The hydroxide/carbonate impurity peak appears to have vanished, which should again not be interpreted in a quantitative manner due to the above-mentioned uncertainty of the fit, but as a trend it is consistent with the decrease of the carbonate and hydroxide bands after SO_3 treatment observed by DRIFTS (Fig. 4).

Table II. Assignment of vibrational frequencies of the relevant species with strong (s), medium (m), weak (w) intensity or shoulder (sh).

Frequency	Assignment	Comments/literature references
Region around 3450 cm^{-1} (2500 to 3600 cm^{-1})	OH^-/H_2O	OH^- stretching vibration[49] at 3575 cm^{-1} Stretching vibration of the hydrate H_2O molecule[49] at 2965 cm^{-1}
1470 cm^{-1} (s)	CO_3^{2-}, HCO_3^-	CO_3 asymmetric stretch[50–54]
1300 cm^{-1} (s)	$S_2O_7^{2-}$	52, 53, 55, 56
1130 cm^{-1}(s)	SO_4^{2-}	SO_4 stretch[51–53,57–60]
1060 cm^{-1} (sh)	SO_4^{2-}, $S_2O_7^{2-}$	51–53, 55–60
1002 (m)	SO_3^{2-}	51, 52, 61
954 (s)	SO_3^{2-}	51, 52, 61
860 cm^{-1}	CO_3^{2-}	CO_3 bending out of plane vibrations[50–53]
820 cm^{-1} (w-m)	$S_2O_7^{2-}$	52, 53, 55, 56
632 (w)	SO_3^{2-}	51, 52, 61
570 cm^{-1} (s)	$Li_{1+x}M_{1-x}O_2$	MO_6 stretch[62–64]

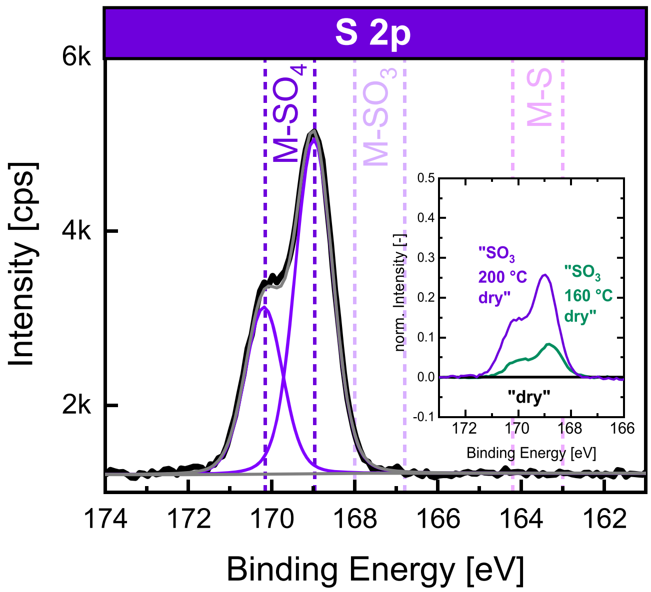

Figure 5. Analysis of the S 2p XPS data of the LMR-NCM material treated in SO_3 gas at 200 °C ("SO_3 200 °C dry"; main figure), with the *y*-axis given in counts per second (cps). Inset: Comparative signal intensities of the dried as-received LMR-NCM ("dry") and of the samples treated with SO_3 gas at different temperatures ("SO_3 160° dry" and "SO_3 200 °C dry") normalized to the intensity at 1200 eV. Background subtraction (data in the inset) was done after normalization.

Impact of wet storage on the surface composition.—We now want to elucidate the effects of LMR-NCM material storage at high relative humidity ambient air ("wet" storage) by additional XPS data. Figure 7 thus depicts O 1s spectra of as-received "calcined" and "wet" LMR-NCM samples in comparison to LMR-NCM treated with SO_3 at 160 °C in "dry" state (same data as mid panel in Fig. 6) as well as after "wet" storage.

When comparing as-received "calcined" and "wet" LMR-NCM (Fig. 7, left panel), the peak representing hydroxide/carbonate impurities is more pronounced after storage of the material at high relative humidity ambient air, which is in line with DRIFTS data (Fig. 4). Comparing the SO_3-treated samples in "dry" and "wet" condition (Fig. 7, right panel), changes in hydroxide/carbonate and sulfate content are within the uncertainty of the fit, so that it is not possible to determine whether the amount of hydroxide/carbonate species has increased upon wet storage. The only significant difference between the two spectra is the appearance of an additional peak at ≈533 eV appearing after "wet" storage (labelled as "misc."), which either points to the formation of a hydrated sulfate or to sodium contamination, as detailed in the supporting information: A comparison of anhydrous nickel sulfate with its hydrate $NiSO_4 \cdot 6\ H_2O$ reveals a signal at ≈533.5 eV for the hydrate (Fig. S2 and Table SI). On the other hand, the XPS survey scan of the "SO_3 160 °C dry" sample clearly shows evidence for the presence of sodium (Fig. S3), presumably from the synthesis process, so that the peak at ≈533 eV could also correspond to the Na_{KLL} Auger line at 533 eV.[73] It is unclear, if both effects play a role or if only one of them causes the additional peak at ≈533 eV for "wet" stored SO_3-treated LMR-NCM.

Effect of surface contaminants on electrolyte stability.—Having discussed the surface composition of SO_3-treated LMR-NCM via DRIFTS and XPS analysis, we now want to investigate the impact of the different LMR-NCM surfaces on the stability of an ethylene carbonate (EC) based electrolyte in contact with the cathode active material at elevated temperature. The following experiment is based on our previous study,[41] where we demonstrated that catalytically active hydroxide ions (OH^-) in the presence of trace amounts of

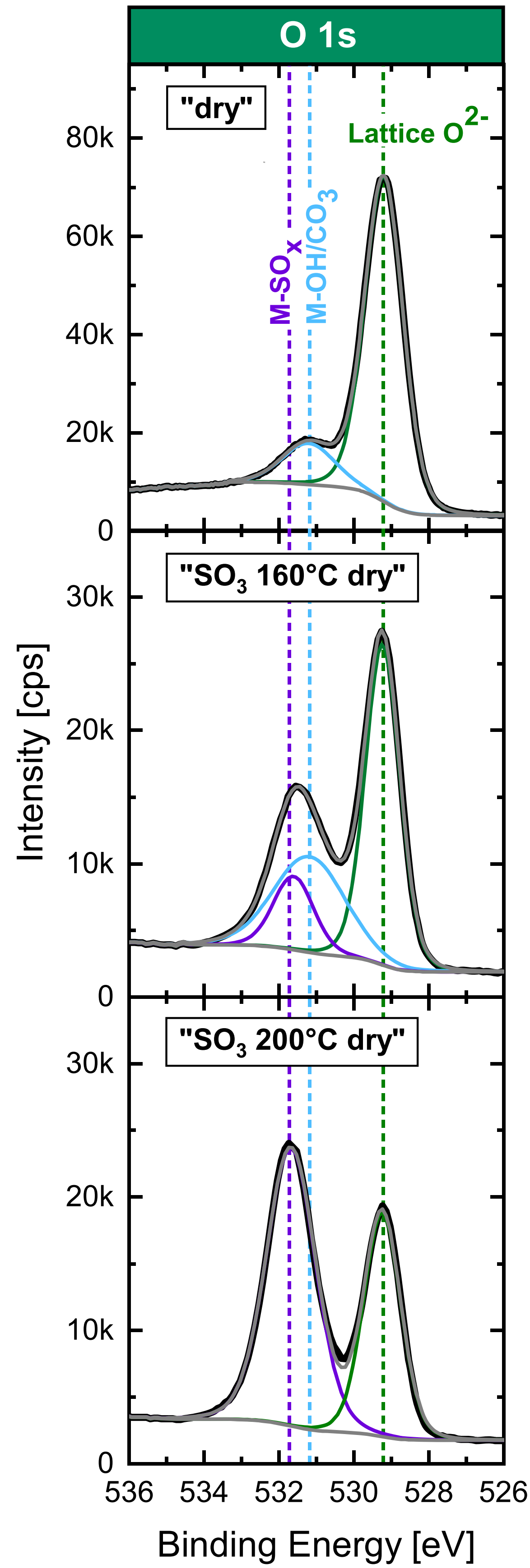

Figure 6. XPS O 1s region for the LMR-NCM samples "dry," "SO_3 160 °C dry" and "SO_3 200 °C dry" (same samples for which the S 2p data are shown in Fig. 5).

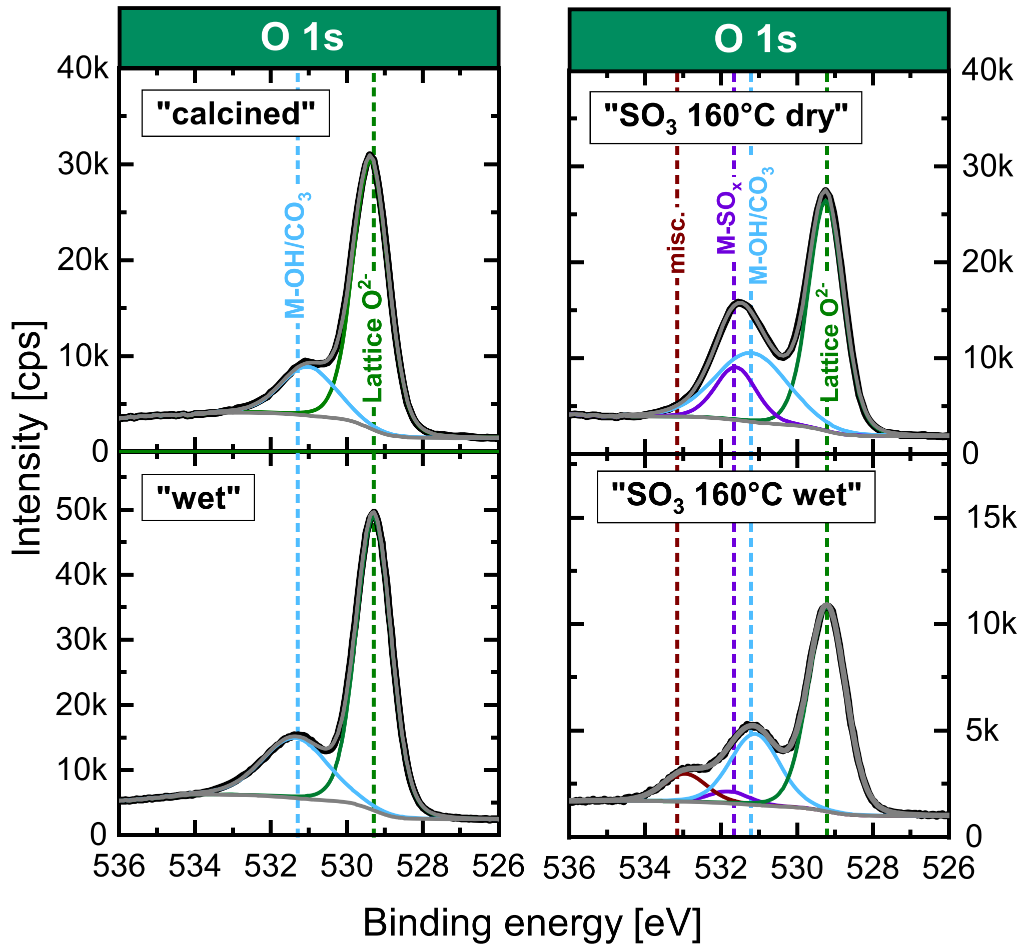

Figure 7. Effect of LMR-NCM material storage at high relative humidity ambient air ("wet" storage, see Fig. 2). O 1 s XPS of as-received "calcined" and "wet" LMR-NCM (left panel) compared to the sample treated with SO_3 at 160 °C without and after exposure to high humidity ambient air ("SO_3 160 °C dry" and "SO_3 160 °C wet," respectively; right panel).

H_2O can lead to a rapid decomposition of EC at the approximately upper temperature limit for lithium-ion battery operation. The decomposition of EC is induced by a nucleophilic attack of OH^-, and a subsequent ring opening reaction of EC under abstraction of CO_2. In a more recent study,[13] we demonstrated that a similar reaction can be triggered by basic surface contaminants like $NiCO_3 \cdot 2\,Ni(OH)_2 \cdot x\,H_2O$. We also showed that this reaction not only leads to the decomposition of EC-based electrolyte and accumulation of CO_2 gas in the battery cell, but also to a deterioration of battery performance.

For this purpose we conducted an on-line mass spectrometry (OMS) test analogous to our previous work,[13,41] exposing a mixture of cathode active material to EC-only electrolyte (EC + 1.5 M $LiClO_4$) at a realistic mass ratio[24] of 0.35:1 at an elevated temperature of 60 °C and following the evolution of CO_2 over time. This EC decomposition experiment only accounts for hydroxide based impurities,[13,41] but not for carbonates such as Li_2CO_3, which does not react with the organic carbonate solvent itself.[74] We mixed 515 mg LMR-NCM with 120 μl EC-only electrolyte; in case of the untreated "calcined" and "dry" samples, 1.03 g cathode active material and 240 μl electrolyte were used to enhance the sensitivity for the expected much smaller amounts of evolved CO_2. The impact of wet storage on gassing was investigated for untreated as well as SO_3-treated LMR-NCM (Fig. 8).

Figure 8a illustrates the cell temperature set points (black line) and the cell temperature profile (red line) in the OMS experiment. First, the CO_2 baseline signal is recorded at 10 °C for 3 h and subsequently a step to 60 °C is applied to trigger the EC decomposition reaction. After 12 h at 60 °C, the total amount of CO_2 has reached ≈56 $\mu mol/g_{EC}$ for the untreated LMR-NCM after a 1 week storage at high relative humidity air ("wet," see Fig. 8b) compared to ≈27 $\mu mol/g_{EC}$ for as-received and dried LMR-NCM ("dry"), which corresponds to an increase by a factor of two. However, with the as-received and calcined LMR-NCM ("calcined"), the CO_2 evolution is drastically reduced, leading to the formation of only ≈9 $\mu mol/g_{EC}$ after 12 h at 60 °C, which is ≈3-fold less than observed for the "dry" sample. It should be noted that for the "dry" sample a different temperature chamber was used which needed slightly more time to reach the 60 °C setpoint temperature (data not shown), so that the initial CO_2 increase is a bit more delayed compared to the other samples. When determining the CO_2 evolution rates from the CO_2 concentration increase over the last hour of the experiment (Fig. 8d), the differences become even more drastic, with an essentially negligible CO_2 evolution rate of ≈$6.6{\cdot}10^{-13}$ $mol_{CO2}/(s{\cdot}g_{EC})$ for the "calcined" LMR-NCN sample compared to ≈$1.7{\cdot}10^{-10}$ and ≈$3.7{\cdot}10^{-10}$ $mol_{CO2}/(s{\cdot}g_{EC})$ for the "dry" and the "wet" samples. The impact of wet storage of cathode active materials on the EC decomposition at elevated temperatures as well as the much reduced degradation after a complete removal of surface contaminants by are-calcination of cathode active materials in combination with a strict avoidance of air exposure has already been described in our previous study with NCM811.[13]

Figure 8c shows the same CO_2 gassing analysis for the LMR-NCM material treated with SO_3 at 160 °C before and after wet storage ("SO_3 160 °C dry" and "SO_3 160 °C wet," respectively). For both cases, the total amount of evolved CO_2 over 12 h at 60 °C is identical (≈7 $\mu mol/g_{EC}$) and also quite similar to the "calcined" sample that was not treated with SO_3 (≈9 $\mu mol/g_{EC}$). Furthermore,

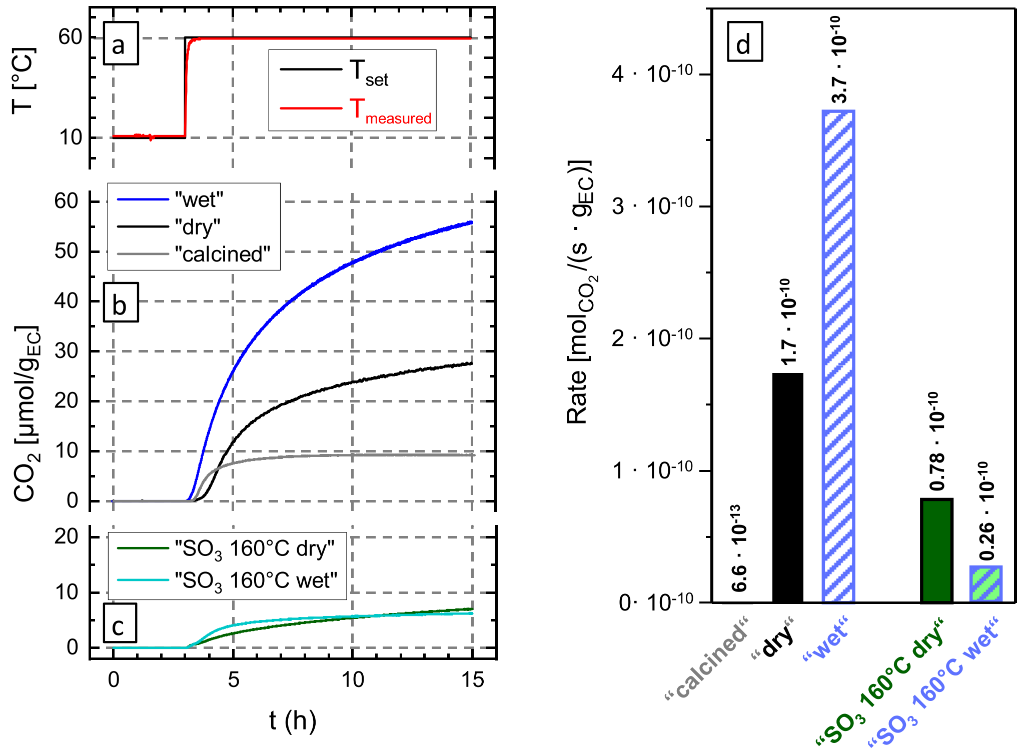

Figure 8. (a) Temperature set point and cell temperature vs time during (b) OMS measurements with mixtures of 120 μl of EC-only electrolyte (1.5 M $LiClO_4$ in EC) with 515 mg of untreated cathode active material in the conditions "wet" (blue line), "dry" (black line) and "calcined" (grey line). The total CO_2 amount is normalized to the mass of electrolyte [$\mu mol_{CO2}/g_{EC}$] (y-axis). (c) The green lines show the CO_2 evolution of LMR-NCM treated with SO_3 at 160 °C before and after wet storage ("SO_3 160 °C dry" and "SO_3 160 °C wet," respectively). (d) The CO_2 evolution rate is determined from the slope (linear fit) of the CO_2 signal in the last hour of the measurement.

the CO_2 evolution rate (Fig. 8d) of the "wet" SO_3-treated sample, appears to be slightly lower than the one of "dry" SO_3-treated material ($\approx 0.26 \cdot 10^{-10}$ compared to $\approx 0.78 \cdot 10^{-10}$ $mol_{CO2}/(s \cdot g_{EC})$), which might be a deviation within the error margin of the method. In summary, the EC hydrolysis experiments demonstrate that the SO_3 treatment leads to a preservation of the low level of hydroxide-based surface contaminants achieved by the prior calcination, even if exposed to excessive moisture.

Cycling of LMR-NCM//graphite cells.—LMR-NCM//graphite coin cells with 30 μl of electrolyte (BASF) using differently pre-treated LMR-NCM samples were subjected to extensive cycling at an elevated temperature of 45 °C. The voltage profiles of the first activation cycle at C/15 are displayed in Fig. 9. The characteristic features, namely the sloping plateau between 3 and 4.4 V as well as the activation plateau at 4.5 V are similar for SO_3-treated as well as untreated LMR-NCM samples, while the first cycle charge and discharge capacities vary. First, the calcination of the as-received LMR-NCM ("calcined") positively impacts the activation charge capacity, resulting in an increased capacity of 365 mAh g^{-1} compared to 340 mAh g^{-1} for as-received and dried LMR-NCM ("dry"). This might be explained by a re-intercalation of lithium from surface impurities into the layered oxide lattice during calcination under oxygen, as reported previously for NCM622.[22]

In contrast, the SO_3-treated samples exhibit a lower capacity of 319 mAh g^{-1} during the first charge. The same holds true for the first discharge, with 252–254 mAh g^{-1} for the SO_3-treated samples compared to 271 mAh g^{-1} for the untreated material and 274 mAh g^{-1} for the calcined one. However, this difference in initial discharge capacity may not be relevant for the practical performance of a battery cell with regards to cycle-life and rate capability, which will be discussed in the following.

From Fig. 10a it can be seen that the 1 C cycling capacity retention is rather similar for the "dry," "calcined," and the 160 °C

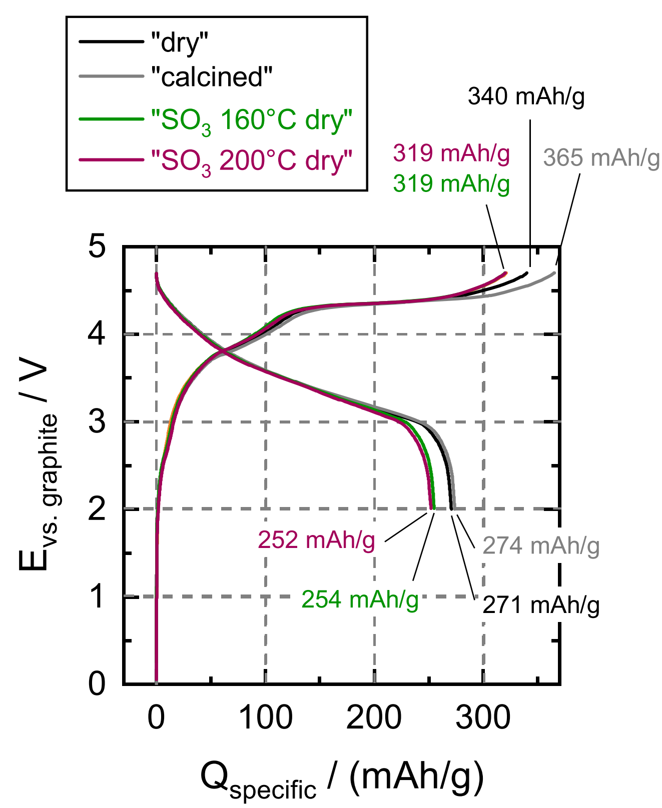

Figure 9. Voltage profiles of LMR-NCM//graphite coin cells for the first activation cycle at 45 °C (4.8 V–2.0 V at C/15). Comparison of SO_3-treated and untreated LMR-NCM. Cell setup and cycling protocol are described in Table I.

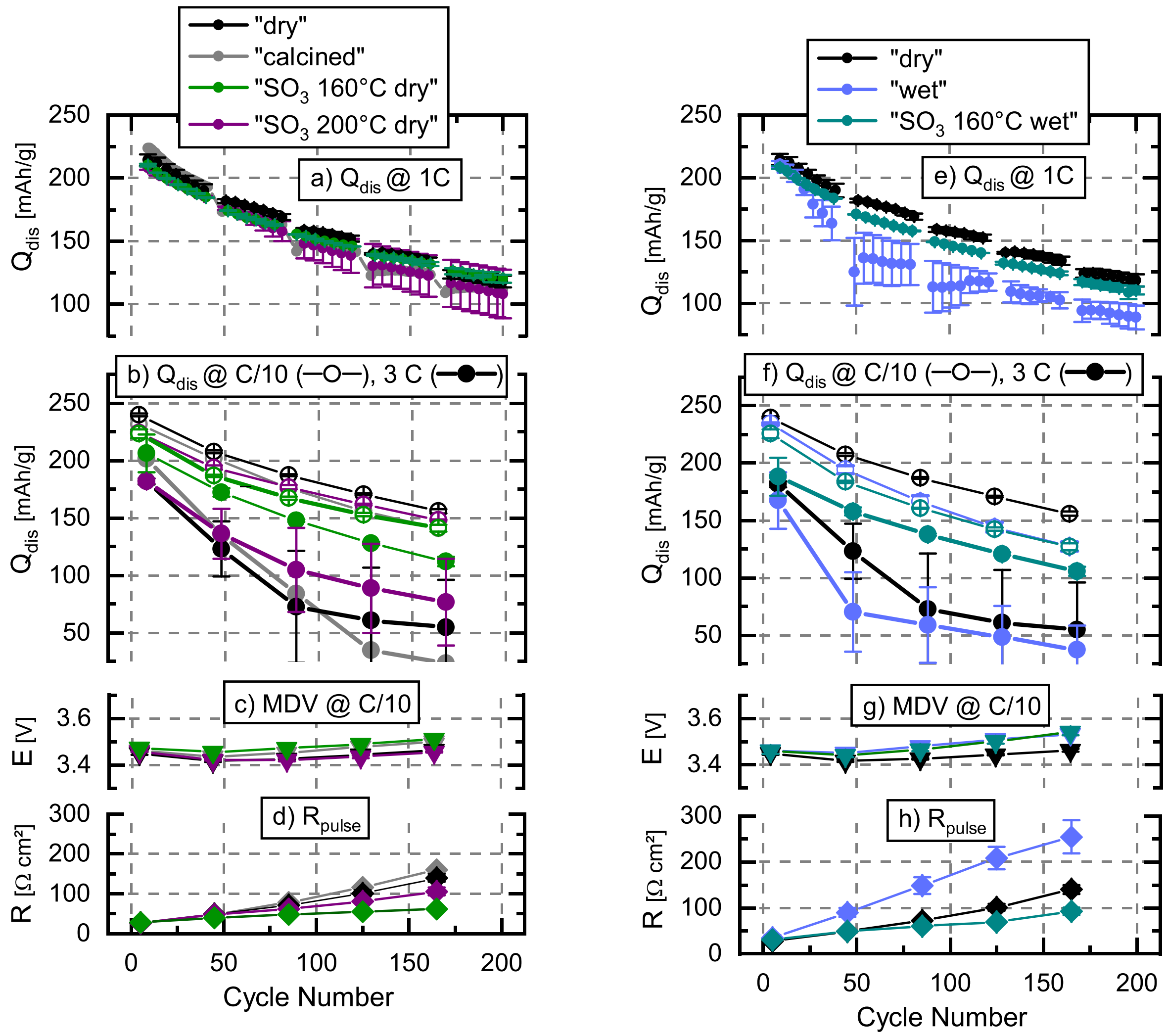

Figure 10. (a)–(d) Impact of SO_3 treatment on full-cell performance of LMR-NCM//graphite coin cells with differently pre-treated LMR-NCMs at 45 °C (average of two cells each, with error bars representing maximum and minimum values). (e)–(f) Effect of a one week long storage at high relative humidity air on SO_3-treated and untreated LMR-NCM materials ("dry" data are the same as in panels (a)–(d)). The various panels show: (a), (e) Discharge capacity (Q_{dis}) at 1 C (only every fifth cycle is displayed for the sake of better visibility); (b), (f) discharge capacity at intermittent cycles at C/10 and 3 C (the last one of the three cycles for every rate is displayed); (c), (g) mean discharge cell voltage (MDV) at C/10; and, (d), (h) DCIR pulse resistance (R) after charge to 40% SOC. The detailed cell setup and cycling protocol are given in the Experimental section and in Table I.

SO_3-treated LMR-NCM materials, while the capacity retention and the cell-to-cell deviation is slightly worse for the "SO_3 200 °C dry" sample, which suggests that the SO_3 treatment at 200 °C is perhaps too harsh. Overall, the discharge capacity at C/10 (Fig. 10b, open circles) is slightly higher for untreated LMR-NCM ("dry" and "calcined") compared to the SO_3-treated samples, which is consistent with a minor loss of active lithium due to sulfation as evidenced by the first-cycle discharge capacity (see Fig. 9). However, while the 3 C rate performance (b, solid circles) of "dry" and "calcined" LMR-NCM is comparable, it is drastically improved by the SO_3 treatment, particularly for the LMR-NCM material treated in SO_3 at 160 °C ("SO_3 160 °C dry"), again indicating that the higher SO_3 treatment temperature and the thus higher extent of M-SO_4 surface groups (see Fig. 5) is disadvantageous. For this reason, the LMR-NCM material treated in SO_3 at 160 °C was chosen for the above OMS experiments to investigate the impact of wet storage on the decomposition rate of EC at 60 °C.

The mean discharge voltage of the LMR-NCM//graphite cells is similar for all LMR-NCM samples (Fig. 10c), which means that the SO_3 treatment did not significantly influence the electrochemical bulk properties and bulk charge/discharge characteristics of the LMR-NCM samples. In contrast, the internal resistance build-up during cycling (measured from 10 s DCIR pulses at 40% SOC) is drastically reduced by the SO_3 treatment (Fig. 10d). In fact, the trend of the thus obtained resistance values is consistent with that observed for the 3 C rate performance (Fig. 10b, solid circles): The "SO_3 160 °C dry" sample has the lowest resistance build-up and consequently the best rate capability.

The key question to be answered in this work is, whether the sulfated LMR-NCM material is more robust against wet storage conditions, as was indicated by the above DRIFTS, XPS, and OMS analysis, and whether this indeed would be reflected in a superior cycling performance after wet storage. The comparison of the extended charge/discharge performance of LMR-NCM//graphite cells with the untreated "dry" and "wet" LMR-NCM samples in Fig. 10 clearly illustrates the adverse effect of wet storage conditions on untreated LMR-NCM in terms of cycle-life (Fig. 10e), rate performance (Fig. 10f), and resistance build-up (Fig. 10h). Only the mean discharge voltage (Fig. 10g) is unaffected by wet storage conditions, which means that surface contaminants do not significantly influence the electrochemical bulk charge/discharge characteristics of the LMR-NCM material. This observation is supported by the electrochemical charge/discharge profiles of the first C/15 cycle shown in Fig. S4 in the supporting information. These voltage profiles are rather similar for "dry" and "wet" LMR-NCM, independent of whether they have been SO_3 treated or not prior to exposure to ambient air at high relative humidity.

In contrast to untreated LMR-NCM, the cycling performance of the SO_3-treated sample is not significantly affected by the wet storage. The capacity retention of the "SO_3 160 °C wet" sample (Fig. 10e, green symbols) is similar to untreated "dry" LMR-NCM (black symbols), which means it is also similar to the "SO_3 160 °C dry" material (compare Fig. 10e). Moreover, the rate capability of the "SO_3 160 °C wet" material is even better than the one of untreated LMR-NCM in dry condition (Fig. 10f), and again similar to the "SO_3 160 °C dry" material (compare Fig. 10f). Finally, the "160 °C SO_3 wet" material has a similar resistance build-up as the "dry" LMR-NCM (Fig. 10h), which is only slightly higher than for the "SO_3 160 °C dry" material (compare Fig. 10d). This dramatic improvement of the storage stability due to SO_3 treatment becomes even more apparent when comparing the resistance build-up of untreated vs 160 °C SO_3-treated LMR-NCM, both in "wet" condition (Fig. 10h).

In summary, the SO_3 treatment at 160 °C renders the LMR-NCM material robust against extended storage at high relative humidity in terms of cycling performance and gassing. It therefore is a powerful protection method for cathode active material particles to allow their storage and handling in ambient atmosphere.

Conclusions

In this study we present a novel, continuous, and scalable procedure for the surface sulfation of LMR-NCM cathode active materials, which can be integrated into the industrial manufacturing process of LMR-NCM and other cathode active materials. It combines SO_3 formation by the established contact process with the subsequent SO_3 treatment of LMR-NCM in a tube furnace directly after the removal of surface contaminants by calcination, or alternatively directly integrated into the cool-down step in the production of LMR-NCM.

We show that this surface treatment leads to the formation of surface sulfate groups. We further demonstrate the positive impact of this surface sulfation on the electrochemical performance of LMR-NCM in full-cells as well as on its robustness towards ambient storage and handling.

In the SO_3 treatment at 160 °C or 200 °C, sulfates are formed on the surface of LMR-NCM, as shown by the surface sensitive spectroscopic analysis techniques DRIFTS and XPS. This sulfate formation is accompanied by a minor loss of active lithium that is evident from the first-cycle charge capacity, which is however overcompensated by positive effects such as increased rate capability, reduced resistance build-up, less gassing, and enhanced storage stability.

We showcase the superior robustness of SO_3-treated LMR-NCM to ambient storage and handling by storing it for one week at high relative humidity ambient air. Finally, measurements with LMR-NCM//graphite full-cells demonstrate that there is no performance loss after wet storage of SO_3-treated LMR-NCM, in contrast to untreated LMR-NCM, which suffers from significant capacity fading if subjected to the same wet storage conditions. Another important aspect is the drastically reduced internal resistance build-up for SO_3-treated LMR-NCM material. In summary, our surface modification approach demonstrated for LMR-NCM is a powerful tool not only to induce robustness against atmospheric moisture and CO_2, but also to enhance the rate capability and thus the power density of layered oxides.

Acknowledgments

The authors thank BASF for financial support of this research through the framework of its Scientific Network on Electrochemistry and Batteries. In particular, we thank Dr. Manuel Mendez, Dr. Markus Hölzle, and Dr. Pascal Hartmann (BASF) for fruitful discussions and helpful advice. We further thank Maximilian Pöverlein for his dedicated work and support of this project during his Bachelor's thesis.

ORCID

Johannes Sicklinger https://orcid.org/0000-0003-2815-993X
Louis Hartmann https://orcid.org/0000-0002-3964-1935
Hubert A. Gasteiger https://orcid.org/0000-0001-8199-8703

References

1. G. E. Blomgren, *J. Electrochem. Soc.*, **164**, A5019 (2017).
2. O. Gröger, H. A. Gasteiger, and J.-P. Suchsland, *J. Electrochem. Soc.*, **162**, A2605 (2015).
3. D. Andre, S.-J. Kim, P. Lamp, S. F. Lux, F. Maglia, O. Paschos, and B. Stiaszny, *J. Mater. Chem. A*, **3**, 6709 (2015).
4. K. G. Gallagher, S. Goebel, T. Greszler, M. Mathias, L. Berkeley, W. Oelerich, D. Eroglu, and V. Srinivasan, *Energy Environ. Sci.*, **7**, 1555 (2014).
5. D.-H. Cho, C.-H. Jo, W. Cho, Y.-J. Kim, H. Yashiro, Y.-K. Sun, and S.-T. Myung, *J. Electrochem. Soc.*, **161**, A920 (2014).
6. J. Kim, Y. Hong, K. S. Ryu, M. G. Kim, and J. Cho, *Electrochem. Solid-State Lett.*, **9**, A19 (2006).
7. H. S. Liu, Z. R. Zhang, Z. L. Gong, and Y. Yang, *Electrochem. Solid-State Lett.*, **7**, A190 (2004).
8. H. Liu, Y. Yang, and J. Zhang, *J. Power Sources*, **162**, 644 (2006).
9. R. Jung, R. Morasch, P. Karayaylali, K. Phillips, F. Maglia, C. Stinner, Y. Shao-Horn, and H. A. Gasteiger, *J. Electrochem. Soc.*, **165**, A132 (2018).
10. T. Teufl, B. Strehle, P. Müller, H. A. Gasteiger, and M. A. Mendez, *J. Electrochem. Soc.*, **165**, A2718 (2018).
11. I. A. Shkrob, J. A. Gilbert, P. J. Phillips, R. Klie, R. T. Haasch, J. Bareño, and D. P. Abraham, *J. Electrochem. Soc.*, **164**, A1489 (2017).
12. S. E. Renfrew and B. D. McCloskey, *J. Am. Chem. Soc.*, **139**, 17853 (2017).
13. J. Sicklinger, M. Metzger, H. Beyer, D. Pritzl, and H. A. Gasteiger, *J. Electrochem. Soc.*, **166**, A2322 (2019).
14. R. Moshtev, P. Zlatilova, S. Vasilev, I. Bakalova, and A. Kozawa, *J. Power Sources*, **81–82**, 434 (1999).
15. J. Paulsen and J. H. Kim, *Patent Application*, WO 2012/107313 A1 (2012).
16. J. Paulsen, H.-K. Park, and Y. H. Kwon, *Patent Application*, US 2019/0224201 A1 (2009).
17. J. Paulsen, H. P. Hong, and J. D. Oh, *Patent Application*, WO 2016/055911 A1 (2016).
18. J. R. Dahn, R. Fong, and U. von Sacken, Pat.US 2,264,201 (1993).
19. D.-H. Kim and J. Paulsen, *Patent Application*, WO 2015/128722 A1 (2015).
20. J. Paulsen, H. P. Hong, and H. S. Ahn, *Patent Application*, WO 2015/036882 A2 (2015).
21. N. V. Faenza, L. Bruce, Z. W. Lebens-Higgins, I. Plitz, N. Pereira, L. F. J. Piper, and G. G. Amatucci, *J. Electrochem. Soc.*, **164**, A3727 (2017).
22. Z. Chen, J. Wang, J. Huang, T. Fu, G. Sun, S. Lai, R. Zhou, K. Li, and J. Zhao, *J. Power Sources*, **363**, 168 (2017).
23. R. Jung, P. Strobl, F. Maglia, C. Stinner, and H. A. Gasteiger, *J. Electrochem. Soc.*, **165**, A2869 (2018).
24. J. Kim, H. Lee, H. Cha, M. Yoon, M. Park, and J. Cho, *Adv. Energy Mater.*, **8**, 1702028 (2018).
25. G. V. Zhuang, G. Chen, J. Shim, X. Song, P. N. Ross, and T. J. Richardson, *J. Power Sources*, **134**, 293 (2004).
26. H.-J. J. Noh, S. Youn, C. S. S. Yoon, and Y.-K. K. Sun, *J. Power Sources*, **233**, 121 (2013).
27. X.-D. Zhang, J.-L. Shi, J.-Y. Liang, Y.-X. Yin, J.-N. Zhang, X.-Q. Yu, and Y.-G. Guo, *Adv. Mater.*, **30**, 1801751 (2018).
28. P. Oh, B. Song, W. Li, and A. Manthiram, *J. Mater. Chem. A*, **4**, 5839 (2016).
29. S. F. Amalraj et al., *Electrochim. Acta*, **97**, 259 (2013).
30. X. Zhang, I. Belharouak, L. Li, Y. Lei, J. W. Elam, A. Nie, X. Chen, R. S. Yassar, and R. L. Axelbaum, *Adv. Energy Mater.*, **3**, 1299 (2013).
31. J. Choi, J. Kim, K.-T. Lee, J. Lim, J. Lee, and Y. S. Yun, *Adv. Mater. Interfaces*, **3**, 4 (2016).
32. T. Shinpuku, H. Tani, R. Otterstedt, and K. Kanao, *Patent Application*, WO/2018/172272 (2018).
33. S.-G. Woo, J.-H. Han, K. J. Kim, J.-H. Kim, J.-S. Yu, and Y.-J. Kim, *Electrochim. Acta*, **153**, 115 (2015).
34. B.-J. Chae and T. Yim, *Mater. Chem. Phys.*, **214**, 66 (2018).
35. H. Sclar et al., *J. Electrochem. Soc.*, **167**, 110563 (2020).
36. M. Metzger et al., *WIPO Pat. Appl. No.*, WO2019002116 (2018).
37. K. Watanabe and M. Deguchi, *Patent Application*, US 2011/0117437 A1 (2011).
38. B. Strehle, K. Kleiner, R. Jung, F. Chesneau, M. Mendez, H. A. Gasteiger, and M. Piana, *J. Electrochem. Soc.*, **164**, A400 (2017).
39. O. B. Lapina, B. S. Bal'zhinimaev, S. Boghosian, K. M. Eriksen, and R. Fehrmann, *Catal. Today*, **51**, 469 (1999).
40. A. F. W. Hollemann and N. Wiberg, "Schwefelsäure H_2SO_4 und Dischwefelsäure $H_2S_2O_7$." *Lehrbuch der Anorganischen Chemie* (de Gruyter, Berlin) p. 583 (2008).
41. M. Metzger, B. Strehle, S. Solchenbach, and H. A. Gasteiger, *J. Electrochem. Soc.*, **163**, A1219 (2016).
42. M. Metzger, C. Marino, J. Sicklinger, D. Haering, and H. A. Gasteiger, *J. Electrochem. Soc.*, **162**, A1123 (2015).
43. F. T. Wagner, B. Lakshmanan, and M. F. Mathias, *J. Phys. Chem. Lett.*, **1**, 2204 (2010).

44. L. D. Ellis, J. P. Allen, L. M. Thompson, J. E. Harlow, W. J. Stone, I. G. Hill, and J. R. Dahn, *J. Electrochem. Soc.*, **164**, A3518 (2017).
45. N. Tsiouvaras, S. Meini, I. H. Buchberger, and H. A. Gasteiger, *J. Electrochem. Soc.*, **160**, A471 (2013).
46. M. Metzger, C. Marino, J. Sicklinger, D. Haering, and H. A. H. A. A. Gasteiger, *J. Electrochem. Soc.*, **162**, A1123 (2015).
47. T. Teufl, D. Pritzl, S. Solchenbach, H. A. Gasteiger, and M. A. Mendez, *J. Electrochem. Soc.*, **166**, A1275 (2019).
48. M. M. Thackeray, C. S. Johnson, J. T. Vaughey, N. Li, and S. A. Hackney, *J. Mater. Chem.*, **15**, 2257 (2005).
49. I. Gennick and K. M. Harmon, *Inorg. Chem.*, **14**, 2214 (1975).
50. P. Pasierb, S. Komornicki, M. Rokita, and M. Rękas, *J. Mol. Struct.*, **596**, 151 (2001).
51. F. A. Miller and C. H. Wilkins, *Anal. Chem.*, **24**, 1253 (1952).
52. R. A. Nyquist and R. O. Kagel, *Handbook of Infrared and Raman Spectra of Inorganic Compounds and Organic Salts: Infrared Spectra of Inorganic Compounds* (New York: Academic, New York) (2012).
53. G. Socrates, *Infrared and Raman Characteristic Group Frequencies: Tables and Charts* (John Wiley & Sons, Inc, New York) (2001).
54. S. Meini, N. Tsiouvaras, K. U. Schwenke, M. Piana, H. Beyer, L. Lange, and H. A. Gasteiger, *Phys. Chem. Chem. Phys.*, **15**, 11478 (2013).
55. R. G. Brown and S. D. Ross, *Spectrochim. Acta Part A Mol. Spectrosc.*, **28**, 1263 (1972).
56. A. Simon and H. Wagner, *Zeitschrift für Anorg. und Allg. Chemie*, **311**, 102 (1961).
57. M. Tatsumisago, H. Narita, T. Minami, and M. Tanaka, *J. Am. Ceram. Soc.*, **66**, c210 (1983).
58. T. Sato, A. Ueno, N. Todo, M. Kurita, H. Hagiwara, A. Nishijima, and Y. Kiyozumi, *Bull. Chem. Soc. Jpn.*, **54**, 3347 (1981).
59. H. Tai and A. L. Underwood, *Anal. Chem.*, **29**, 1430 (1957).
60. S. M. Teleb, *Thermochim. Acta*, **228**, 131 (1993).
61. J. C. Evans and H. C. Bernstein, *Can. J. Chem.*, **33**, 1270 (1955).
62. S. Dasgupta and A. P. B. Sinha, *Trans. Faraday Soc.*, **53**, 909 (1957).
63. R. K. Moore and W. B. White, *J. Am. Ceram. Soc.*, **53**, 679 (1970).
64. C. Julien, *Solid State Ionics*, **135**, 121 (2000).
65. H. Beyer, S. Meini, N. Tsiouvaras, M. Piana, and H. A. Gasteiger, *Phys. Chem. Chem. Phys.*, **15**, 11025 (2013).
66. B. C. Smith, "Diffusive reflectance (DRIFTS)." in*Fourier Transform Infrared Spectroscopy* (CRC Press, Boca Raton, FL) pp. 110 (1996).
67. N. Andreu, D. Flahaut, R. Dedryvère, M. Minvielle, H. Martinez, and D. Gonbeau, *ACS Appl. Mater. Interfaces*, **7**, 6629 (2015).
68. P. van der Heide, "Spectral interpretation." in*X-ray Photoelectron Spectroscopy : An Introduction to Principles and Practices*, ed. P. van der Heide (John Wiley & Sons, Inc, Hoboken, NJ, United States of America) pp. 101 (2011).
69. M. C. Biesinger, B. P. Payne, A. P. Grosvenor, L. W. M. Lau, A. R. Gerson, and R. S. C. Smart, *Appl. Surf. Sci.*, **257**, 2717 (2011).
70. A. R. Gonzalez-Elipe, J. P. Espinos, A. Fernandez, and G. Munuera, *Appl. Surf. Sci.*, **45**, 103 (1990).
71. M. C. Biesinger, B. P. Payne, L. W. M. Lau, A. Gerson, and R. S. C. Smart, *Surf. Interface Anal.*, **41**, 324 (2009).
72. J.-C. Dupin, D. Gonbeau, P. Vinatier, and A. Levasseur, *Phys. Chem. Chem. Phys.*, **2**, 1319 (2000).
73. A. Gutierrez, M. He, B. T. Yonemoto, Z. Yang, J. Wang, H. M. Meyer, M. M. Thackeray, and J. R. Croy, *J. Electrochem. Soc.*, **166**, A3896 (2019).
74. A. T. S. Freiberg, J. Sicklinger, S. Solchenbach, and H. A. Gasteiger, *Electrochim. Acta*, **346**, 136271 (2020).